

Studies of transverse and longitudinal relaxations of ^{55}Mn in molecular cluster magnet Mn_{12}Ac

Takao Goto* and Takeshi Koshihata†

Graduate School of Human and Environmental Studies, Kyoto University, Kyoto 606-8501, Japan

Takeji Kubo

Physics Department, Faculty of Education, Nara University of Education, Nara 630-8301, Japan

Kunio Awaga

Department of chemistry, Graduate School of Science, Nagoya University, Nagoya, 464-0814, Japan

(Dated: October 22, 2018)

The nuclear magnetic relaxation times T_2 and T_1 of ^{55}Mn in the molecular cluster magnet Mn_{12}Ac have been measured, using the spin-echo method for oriented powder sample, at low temperatures below 2.5 K down to 200 mK in the fields up to 9 T applied along the c -axis. Above about 1.5 K both of relaxation rates T_2^{-1} and T_1^{-1} exhibit remarkable decreases with decreasing temperature in zero field with the relative relation like $T_2^{-1}/T_1^{-1} \approx 200$. At the lower temperatures, T_2^{-1} tends to become constant with the value of about 10^2 s^{-1} , while T_1^{-1} still exhibits an appreciable decrease down to around 0.5 K. The analysis for the experimental results was made on basis of the concept that the fluctuating local field responsible for the nuclear magnetic relaxation is caused by thermal fluctuations of the Zeeman levels of the cluster spin of $S = 10$ due to the spin-phonon interactions. Then the problem was simplified by considering only the thermal excitation from the ground state to the first excited state, that is, a step-wise fluctuation with respective average life times τ_0 and τ_1 . By applying nonlinear theory for such a fluctuating local field, a general expression for T_2 was obtained. It turned out that the experimental results for T_2^{-1} are explained in terms of the equation of $T_2^{-1} = \tau_0^{-1}$, which corresponds to the strong collision regime under the condition $\tau_0 \gg \tau_1$. On the other hand, the results for T_1 have been well understood, on the basis of the standard perturbation method, by the equation for the high-frequency limit like $T_1^{-1} \sim 1/\tau_0\omega_N^2$, where ω_N is the ^{55}Mn Larmor frequency. The experimental results for the field dependence of the T_2^{-1} and T_1^{-1} were also interpreted reasonably in terms of the above theoretical treatment. The quantitative comparison between the experimental results and the theoretical equations was made using hyperfine interaction tensors for each of three manganese ions determined from the analysis for the NMR spectra in zero field.

PACS numbers: 75.50.Xx, 76.60.-k, 75.45.+1

Keywords: Molecular magnet Mn_{12}Ac , ^{55}Mn NMR, Relaxation times T_1 and T_2

I. INTRODUCTION

Recently there has been a great interest in nano-scale molecular cluster magnets in view of the microscopic quantum nature appearing in the macroscopic properties of the system. The synthesis of the molecular cluster magnets have solved the most serious problem of the particle size, because the cluster size of the cluster magnet is exactly same and known. As a typical candidate compound, the molecular cluster magnet $\text{Mn}_{12}\text{O}_{12}(\text{CH}_3\text{COO})_6(\text{H}_2\text{O})_4$ (abbreviated as Mn_{12}Ac), which was synthesized and whose crystal structure was studied using X-ray diffraction by Lis,¹ has been studied so far most extensively. Magnetic properties of Mn_{12}Ac have been explained satisfactorily by treating the strongly-coupled cluster spins as a single quantum spin of $S=10$. The prominent features have been demonstrated in very long relaxation time of the magnetization at low temperatures,^{2,3} and the step-wise recovery of the magnetization in the external field at every interval of about 0.45 T, which is associated with the quantum tunneling which occurs with coincidence in the Zeeman

levels of oppositely directed magnetization of the cluster spins.^{4,5} Such a tunneling phenomenon was interpreted as thermally-assisted and/or field-tuned processes associated with the spin-phonon interaction.⁶

Another molecular compound $[(\text{tacn})_6\text{Fe}_8\text{O}_2(\text{OH})_{12}]^{8+}$ (abbreviated as Fe_8) with a large cluster-spin of $S=10$ has been the subject of investigations on the same viewpoint.^{7,8} On contrary to Mn_{12}Ac and Fe_8 in which the tunneling is due to “spin-bath”, a molecular cluster magnet $\text{K}_8[\text{V}_{15}^{\text{IV}}\text{As}_6\text{O}_{42}(\text{H}_2\text{O})]\cdot 8\text{H}_2\text{O}$ (so called V_{15}) has been studied as a system with a lowest cluster spin of $S=1/2$, which shows a hysteresis curve associated with “phonon-bath”, although there is no energy barrier against the spin reversals.⁹

A great deal of experimental and theoretical works related to Mn_{12}Ac has been reviewed in some books and review papers.^{10,11,12,13,14}

In order to understand the magnetic properties of these molecular cluster magnets more thoroughly, it is worthwhile to examine the dynamical behavior as well as statistical nature of each magnetic ion which constitutes the cluster spin. One of the most promising experimental

procedures for this purpose will be to use an NMR with respect to the relevant magnetic ions. In view of this, we have been studying ^{55}Mn NMR in Mn_{12}Ac . As reported in our preliminary paper, we first succeeded, using powder sample, in observing all of ^{55}Mn NMR signals belonging to Mn^{4+} and two in-equivalent Mn^{3+} ions in zero field, and measured the temperature dependence of the transverse relaxation time T_2 at liq. Helium temperatures.¹⁵ In the recent paper, we have determined the hyperfine interaction tensors of ^{55}Mn nuclei in Mn_{12}Ac by analyzing the more detailed ^{55}Mn NMR spectra on the basis of the ground-state spin-configuration.¹⁶

In the present work, we have measured, using oriented powder sample, the transverse relaxation time T_2 and the spin-lattice relaxation time T_1 of ^{55}Mn in Mn_{12}Ac . The measurements have been done in the wide temperature range from 2.5 K down to 200 mK in zero field and at liq. Helium temperatures with an applied field up to 9 T. As for the nuclear-spin lattice relaxation in Mn_{12}Ac , the proton spin- and muon spin-lattice relaxation times have been measured by Lascialfari *et al.* at the temperature range of 4.2–400 K and at the field range of 0–9.4 T,¹⁷ and subsequently at the lower temperatures down to around 2 K below 1.6 T.¹⁸ In Ref. 18 the field dependence of the proton relaxation rate T_1^{-1} and the temperature dependence of the muon relaxation rate have been analyzed on the basis of the standard perturbation method, that is, weak collision model. Then the fluctuating local fields at the proton or the muon site have been taken to originate from the random change between the adjacent Zeeman-energy levels of the ground-state configuration of the total spin of $S=10$, which is caused by the spin-phonon interactions. Quite recently Furukawa *et al.* have reported on the experimental results for the temperature and field dependence of T_1^{-1} of ^{55}Mn in Mn_{12}Ac above 1.2 K and below 1 T,¹⁹ and the analysis has been made on the basis of essentially the same treatment given in Ref. 18.

The analysis for our experimental results are made on the basis of the concept as presented in Ref. 18 such that the fluctuating local field at each of ^{55}Mn sites in Mn^{4+} and Mn^{3+} ions is originated from the thermal excitations in the Zeeman-energy levels due to the spin-phonon interaction. Then, in order to proceed the analytical treatment, we simplify the problem by taking into account only the lowest two levels of the cluster spin $S=10$, the ground-state and the first excited state which lies above about 12 K. This simplification will be reasonable, since the data for the ^{55}Mn NMR are available only below about 2.5 K, thus the statistical weight of higher excited states being extremely small. For the interpretation for T_2 , which was measured by observing the spin-echo decay time, we employ the general treatment based on non-linear theory. As we shall explain, it turns out that the transverse relaxation rate T_2^{-1} is reasonably understood in terms of the strong collision regime instead of weak collision regime. On the other hand, the results of T_1 is interpreted satisfactorily by the standard perturbation

formalism. However, our standpoint for the interpretation for T_1 is somewhat different from that presented in Ref. 19 apart from the simplification of the problem. The essential part has already been reported in our recent brief publication.²⁰

The constitution of the present article is as follows. In the next section, we explain briefly the magnetic structure and hyperfine coupling tensors of ^{55}Mn in Mn_{12}Ac determined by analysis of ^{55}Mn NMR spectra. The experimental results are presented in Sec. III. Section IV is devoted to the derivation of the theoretical equations for interpretations for the experimental results. Subsequently we show that the experimental results of T_2 and T_1 are interpreted reasonably in terms of the present theoretical treatment. In Sec. V we discuss on the quantitative considerations. The final section yields the summaries of this article.

II. PROPERTIES OF Mn_{12}Ac

A. Crystal Structure and magnetic properties

The crystal and magnetic structures of the cluster of Mn_{12}Ac are shown in Fig. 1(a). Each cluster, which constitutes a tetragonal symmetry with the lattice constants of $a = b = 17.3 \text{ \AA}$, and $c = 12.4 \text{ \AA}$, is constructed from four Mn^{4+} ions ($S = 3/2$) in a central tetrahedron (denoted by Mn(1)) and surrounding eight Mn^{3+} ($S = 3/2$) with two in-equivalent sites (denoted by Mn(2) and Mn(3)) located alternately. The Mn atoms are linked by triply bridged oxo oxygens and by carboxylate bridges from acetate anions. The Mn(1) and Mn(2) have distorted octahedral coordination of oxygens due to above links. In Mn(3), one water molecule completes the octahedral environment of oxygens.¹

There exist four kinds of exchange interactions among these manganese ions, as shown schematically in Fig. 1(b). Quite recently, a set of the magnitudes and signs of these exchange couplings has been determined, using exact diagonalization of the spin Hamiltonian of the cluster spin by a Lanczos algorithm, so as to explain the high-field magnetization and the realization of the ground state of $S = 10$. These values are $J_1/k_B = -119 \text{ K}$, $J_2/k_B = -118 \text{ K}$ (antiferromagnetic), $J_3/k_B = 8 \text{ K}$ (ferromagnetic) and, $J_4/k_B = -23 \text{ K}$,²³ and except the value of J_1/k_B , they are different largely from the previously available values.²¹

As a combined effect of the above exchange interactions, the ground-state configuration of the total spin of $S = 10$ is established²² in such a way that the assemblies of outer eight Mn^{3+} ions and the inner Mn^{4+} ions, which have respectively resultant ferromagnetic spins of $S = 16$ (8×2) and $S = 6$ ($4 \times 3/2$), are coupled antiferromagnetically to each other at low temperatures.²² Because of the anisotropy due to Jahn-Teller distortion of Mn^{3+} ions, there appears a single-ion type anisotropy D along the $\pm c$ -axis. Thus the total magnetic moments

of each cluster are either parallel or anti-parallel to the c -axis. Henceforth these clusters are referred to respectively as (+) and (-) cluster, with respect to the c -axis taken as the z -axis. The inter-cluster interaction is only due to dipolar origin of the order of 0.5 K. In the presence of an external field H_0 applied along the c -axis, the effective exchange Hamiltonian for each cluster is given by

$$\mathcal{H} = -DS_z^2 - BS_z^4 \pm g_{\parallel}\mu_B H_0 S_z, \quad (1)$$

where the exchange parameters have been evaluated from recent high-field ESR²⁴ and neutron spectroscopy²⁵ as $g_{\parallel} = 1.93$,²⁴ $D/k_B = 0.67$ K,²⁴ and 0.66 K,²⁵ and $B/k_B = 1.1-1.2 \times 10^3$ K,²⁴ and the sign \pm correspond to the (+) and (-) clusters, respectively. According to this Hamiltonian, the discrete energy levels $|S, m\rangle$ are well defined along the z -axis in the ground-state spin configuration of $S = 10$. This gives satisfactory understandings for the most of magnetic properties of Mn_{12}Ac such as an energy barrier of about 60 K in zero field from the ground level of $m = \pm 10$ up to the highest level of $m = 0$, and the step-wise recovery of the magnetization at each step of about 0.45 T which occurs corresponding to the coincidence of the energy levels between $S_z = m(< 0)$ in the (+) cluster and $S_z = m(> 0)$ in the (-) cluster. In addition to the above main Hamiltonian, there exists the perturbing Hamiltonian \mathcal{H}' including the terms such as higher-order transverse anisotropy and the transverse external field. These terms do not commute with S_z , thus playing a crucial role for the mechanism of the tunnelling. In particular, the transverse external field gives rise to a drastic change in the tunnel-splitting at the level-crossing fields, which may promote the tunneling appreciably.²⁶

B. Hyperfine interaction tensor

Next we review the ^{55}Mn hyperfine interaction tensor determined from the NMR spectra in zero field in Ref. 16 for the numerical evaluation of the present experimental results. Figure 2 shows the NMR spectra of ^{55}Mn ($I = 5/2$) in Mn_{12}Ac obtained at 1.45 K in zero field. The three completely separated lines with the central frequencies of $\nu_N = 230, 279$, and 364 MHz, were identified to be due to Mn^{4+} ion ($\text{Mn}(1)$), and Mn^{3+} ion ($\text{Mn}(2)$ and $\text{Mn}(3)$), respectively. The corresponding internal fields are $H_{\text{int}} = 21.8, 26.5, 34.5$ T. From now on, these three lines are referred to as L1, L2, and L3, respectively. The resonance lines L1, L2, and L3 involve the five-fold quadrupole-splitting with $\Delta\nu_q = 0.72, 4.3, 2.9$ MHz, respectively.¹⁶

The nuclear hyperfine Hamiltonian, which consists of Fermi-contact, dipolar, and orbital terms, is obtained by taking the expectation values for the corresponding Hamiltonians with respect to the ground-state wavefunction of the magnetic ion. This Hamiltonian is expressed as,

$$\mathcal{H}_N = \mathbf{I} \cdot \mathbf{A} \cdot \mathbf{S} = -\gamma_N \hbar \mathbf{I} \cdot (\mathbf{H}_F + \mathbf{H}_d + \mathbf{H}_l), \quad (2)$$

where \mathbf{A} is the hyperfine coupling tensor between the nuclear spin \mathbf{I} and the electronic spin \mathbf{S} , and \mathbf{H}_F , \mathbf{H}_d , \mathbf{H}_l are the corresponding hyperfine fields. Each of manganese ions in Mn_{12}Ac is subject to the crystalline field with dominant cubic symmetry due to the surrounding distorted octahedral coordination of oxygens.

The ground-state of the Mn^{4+} ion ($3d^3$, 4F) is the orbital-singlet. So the dipolar and the orbital terms in Eq. (2) vanishes primarily, and only the isotropic Fermi-contact term is important. The corresponding Fermi-contact field \mathbf{H}_F is given, using the conversion factor of 1 atomic unit ($a.u.$) = 4.17 T, as

$$\mathbf{H}_F = -\frac{A_f \mathbf{S}}{\gamma_N \hbar} = -2 \times 4.17 \chi \mathbf{S}, \quad (3)$$

where A_f is the component of the tensor \mathbf{A} , and χ is the effective field per unpaired electron in atomic unit. According to Freeman and Watson,²⁷ the value of χ is calculated to be 2.34 for the free Mn^{4+} ion, by taking into account the contributions from three inner electron spins ($1s$, $2s$, and $3s$). The minus sign in \mathbf{H}_F indicates that the direction of \mathbf{H}_F is opposite to the magnetic moment. Thus for the free Mn^{4+} ion, the values of \mathbf{H}_F is estimated to be $H_F = 29.3$ T. The effect of the admixture of the higher triplet state to ground-state and distorted crystalline field may be extremely small. In fact, for the diluted ion in the trigonal symmetry, the hyperfine anisotropy is of the order of 0.1%.²⁷ It is noted that the experimental internal field of 21.8 T is smaller by 26% as compared with calculated value of 29.3 T for the free ion. This is understood by considering a large amount of reduction of the magnetic moment. The recent polarized neutron diffraction measurement yields the presence of 22% reduction from the full value of $3\mu_B$ in the magnitude of the Mn^{4+} magnetic moment.²⁸ Since the reduction of the magnetic moment due to $3d$ -electrons reflects the contact term, the present result is consistent with the neutron results. Such a large amount of reduction may be ascribed to the presence of the covalence and strong exchange interactions, as observed usually in the condensed matter.

On the other hand, the ground state of the Mn^{3+} ion ($3d^4$, 5D) is orbital doublet denoted by E_g in the cubic crystalline field. As in the case of Mn^{4+} ion, the Fermi-contact field $H - F$ is obtained for the free Mn^{3+} to be 48.5 T using the calculated value of $\chi = 2.91$.²⁷ Because of the additional elongated tetragonal symmetry of the crystalline field caused by Jahn-Teller effect and low-symmetric carboxylate ligands, the orbital degeneracy is removed to the lower and higher states with the wave functions expressed as $|\Psi_1\rangle = |X^2 - Y^2\rangle$ and $|\Psi_2\rangle = |3Z^2 - r^2\rangle$, respectively. Here we defined the rectangular coordinate system (XYZ) with the tetragonal Z -axis and the X -axis along one of the principal axes in the tetragonal plane. Further, the orthorhombic distortion of the crystalline field gives rise to the admixture of $|\Psi_2\rangle$ to $|\Psi_1\rangle$, thus the ground-state wavefunction being expressed as $|\Psi_g\rangle = \cos\phi|\Psi_1\rangle + \sin\phi|\Psi_2\rangle$, where

$\cos\phi$ and $\sin\phi$ are normalization factors. In Mn(2) and Mn(3), the Z -axis tilts from the $c(z)$ -axis by the angles of $\theta = 11.7^\circ$ and 36.2° , respectively. In the case of Mn^{3+} ion, the dipolar term in Eq. 2 contributes appreciably to the hyperfine tensor in addition to the dominant isotropic Fermi-contact term. By using the wave function $|\Psi_g\rangle$ in the standard operator-equivalent method, the dipolar Hamiltonian $\mathcal{H}_d = -\gamma_N \hbar \mathbf{I} \cdot \mathbf{H}_d$, which is expressed in terms of the principal terms with respect to the (XYZ) coordinate system, is given as,

$$\mathcal{H}_d = h_d \gamma_N \hbar \cos(2\phi) \left[S_Z I_Z - \frac{1}{2}(S_X I_X + S_Y I_Y) \right] \quad (4)$$

with

$$h_d = \frac{4}{7} \mu_B \langle r^{-3} \rangle_d,$$

where $\langle r^{-3} \rangle_d$ is the average for the orbital radius r with respect to $3d$ shell. It is useful to define the (xyz) rectangular coordinate system with the z -axis along the magnetic moment and the x -axis is taken in the Zz -plane. (See Fig. 4 in Ref. 16.) Then the above equation is expressed as¹⁶

$$\mathcal{H}_d = \mathbf{I} \cdot \mathbf{D} \cdot \mathbf{S}$$

with

$$\mathbf{D} = \frac{h_d}{4} \gamma_N \hbar \cos(2\phi) \begin{pmatrix} 2(2 - 3 \cos^2 \theta) & 0 & -3 \sin 2\theta \\ 0 & -2 & 0 \\ -3 \sin 2\theta & 0 & 2(3 \cos^2 \theta - 1) \end{pmatrix}. \quad (5)$$

The principal terms are anisotropic, and there appear the off-diagonal terms. For the free Mn^{3+} ion which has $\langle r^{-3} \rangle_d = 4.8 \text{ a.u.}$,²⁷ h_d is evaluated to be $+17.1 \text{ T}$.

The orbital contribution is in general evaluated from the equation, $H_l = -2\mu_B \langle r^{-3} \rangle_d \Delta g$, where Δg represents the deviation of the g -value from $g_s = 2.0023$ due to admixture of the higher excited orbital state. Applying the value of $g_z = 1.95$ and $g_\perp = 1.97$ for Mn^{3+} ion evaluated from high field EPR measurement,²⁴ the value of H_d is calculated, using $\langle r^{-3} \rangle_d = 4.8 \text{ a.u.}$ for the free ion, to be about 2 T . So, we may neglect the orbital contribution as compared with the other terms. By taking into account the dipolar contribution to the internal field, which is given by the D_{zz} component in the dipolar tensor \mathbf{D} (Eq. (5)), the total internal field is given by

$$H_{\text{int}} = |\mathbf{H}_F| - D_{zz} / \gamma_N \hbar. \quad (6)$$

The identification of the L2 and L3 lines was made in view of Eq. (6). By considering that the increase in θ plays a role to deduce $|\mathbf{H}_F|$ as far as $\theta < 53^\circ$, it turns out that the line L2 with lower ω_N should be due to Mn(2), and thus the L3 line being due to Mn(3). As for the quadrupole splitting, the dominant term is expressed, for the axial-symmetry case, as $\Delta\nu_q = \frac{1}{2}(3 \cos^2 \theta - 1)\nu_q$, where ν_q is the quadrupole-splitting parameter. The larger value

of θ yields the larger splitting as far as $\theta < 53^\circ$. The above identification is then consistent with the observed difference in quadrupole splitting between ^{55}Mn NMR for the L2 and L3 lines.

The determination of the components of the hyperfine tensors A for Mn(2) and Mn(3) of Mn^{3+} ion was made in the following way. There are three unknown factors, the reduction factor for the contact term, the value of $\langle r^{-3} \rangle_d$, and the amount of the mixing of the two wave functions in the ground-state E_g , which is represented by the factor $\cos 2\phi$ in Eq. (5). According to Ref. 28, the reductions of the magnetic moments for the Mn(2) and Mn(3) ions are obtained to be 8% and 6%, respectively. First, by applying these reduction factors to the value of $\langle r^{-3} \rangle_d$ in Eq. (4) for each ion, we evaluated that $h_d = +15.7$ and $+16.0 \text{ T}$, respectively. Secondly, referring to the crystal parameters given in Ref. 1, we assumed the tetragonal and orthorhombic symmetries of the crystalline field for Mn(2) and Mn(3), respectively. That is, we put $\cos 2\phi = 1$ for Mn(2), and the coefficient $\cos 2\phi$ for Mn(3) was remained as an unknown factor. Then using $\theta = 11^\circ$ for Mn(2), we obtain the dipolar contribution $D_{zz} / \gamma_N \hbar = +1.6 \text{ T}$. Using the experimental value of 26.5 T for H_{int} in Eq. (6), we find $H_F(\text{Mn}(2)) = 24.8 \text{ T}$. This corresponds to 85% of H_{int} for the free ion, thus reduction factor for the contact term being evaluated to be 15%. Next we adopted the same value of the contact field for Mn(3). Then using $\theta = 36^\circ$, the mixing parameter for Mn(3) was estimated to be $\cos 2\phi = 0.89$. From the above considerations, we finally determined the following numerical values of the components of the ^{55}Mn hyperfine-interaction tensors for each of three manganese ions, which are expressed in unit of MHz with respect to the (xyz) -coordinate frame with the z -axis of the c -axis;

$$A(\text{Mn}(1)) = \text{diag}(153, 153, 153), \quad (7a)$$

$$A(\text{Mn}(2)) = \begin{pmatrix} 254 & 0 & -24.7 \\ 0 & 176 & 0 \\ -24.7 & 0 & 140 \end{pmatrix}, \quad (7b)$$

$$A(\text{Mn}(3)) = \begin{pmatrix} 221 & 0 & -53.0 \\ 0 & 181 & 0 \\ -53.0 & 0 & 182 \end{pmatrix}. \quad (7c)$$

III. EXPERIMENTAL RESULTS FOR THE RELAXATION RATES

The transverse and longitudinal relaxation times T_2 and T_1 of the ^{55}Mn were measured for the three resonance lines at the liq. Helium temperatures with the external field H_0 up to 9 T applied along the c -axis, and for the L1 line the measurement was extended down to 200 mK in zero field. Figure 3 shows the field dependence of the resonance frequencies of the central peaks of the three resonance lines, which was obtained at 1.65 K by applying the external field H_0 along the c -axis (z -axis) after zero-field cooling. Within the experimental error, the

slopes of these lines coincide with the gyromagnetic ratio γ_N of the free manganese nuclei. As explained in Sec. II B, the internal field H_{int} of ^{55}Mn , which is mainly due to the Fermi-contact term, appears along the spin direction, that is, opposite to the magnetic moment. So when $H_{\text{int}} \gg H_0$ as in the present case, the resonance conditions for Mn^{4+} ion belonging to the (+) and (-) clusters are given by $\omega_N = \gamma_N(H_{\text{int}} \pm H_0)$, and these are referred to as upper and lower branches, respectively. In the case of Mn^{3+} ion, the above relations are vice versa.

At lower temperatures than the blocking temperature of $T_B \approx 3\text{ K}$, we can observe the NMR signals and measure T_2 and T_1 for the (-) cluster in addition to those for the (+) cluster, as far as the relaxation time of the reorientation of the (-) clusters to the z -direction is enough longer as compared with T_1 . The transverse relaxation time T_2 were obtained by measuring the decay of spin-echo amplitude as a function of the time interval between two rf -pulses. The decay was of single-exponential type. The longitudinal relaxation time T_1 is obtained in general by measuring the recovery of the nuclear magnetization after the saturation of the nuclear magnetization of the central line. Under the ideal condition of the complete saturation, the magnetization recovery for the nucleus of $I = 5/2$ is obtained by the equation²⁹

$$m(t) = 1 - \frac{M(t)}{M_0} \\ = a \exp(-t/T_1) + b \exp(-6t/T_1) + c \exp(-15t/T_1) \quad (8)$$

with the condition such that $a + b + c = 1$. However, in the present case, it was difficult to attain complete saturation of the NMR signal because of the broadness of each quadrupole splitting resonance line. Then the relaxation rate T_1 was determined by doing the best-fitting of the experimental recovery curve to the Eq. (8). The value of T_1 obtained in such a way was almost the same as the value determined from the fitting of the slowest recovery region to the single exponential equation $\exp(-t/T_1)$. Figure 4 shows a typical example of the best-fit recovery curve of the nuclear magnetization for the Mn^{4+} ion.

Figure. 5 show the temperature dependence of the transverse relaxation rate T_2^{-1} and the longitudinal relaxation rate T_1^{-1} measured in zero field for each central peak of the three resonance lines. As is seen, both rates exhibit qualitatively the same remarkable decrease with decreasing temperature above about 1.4 K, and the values of T_1^{-1} are smaller than that of T_2^{-1} by almost two orders of magnitudes. Below 1.4 K, T_2^{-1} becomes rather moderate, and it becomes almost constant around the value of 100 s^{-1} below about 0.5 K. The values of T_2^{-1} for Mn^{4+} ion and Mn^{3+} ions are almost the same, though the former is somewhat smaller only at the temperatures above about 2 K. On the other hand, the value of T_1^{-1} continues to decrease remarkably down to around 0.5 K. Thus, at very low temperatures there appears, between T_2^{-1} and T_1^{-1} , a difference extending over four orders of

magnitude. The values of T_1^{-1} for Mn^{3+} ion are larger by about twice than that for Mn^{4+} ion.

The field dependence of T_2^{-1} for $\text{Mn}(1)$, $\text{Mn}(2)$, and $\text{Mn}(3)$. Mn^{4+} ion was measured at 1.65 K for the (+) cluster (upper branch) up to 9 T and for the (-) cluster (lower branch) up to 1.2 T. The data were taken also at 1.45 K only for the (+) cluster up to 9 T. The field dependence of T_1^{-1} for Mn^{4+} ion was measured at 1.65 K for the (+) cluster (upper branch) up to 5 T, and for the (-) cluster (lower branch) up to 1.2 T. The data were taken also at 1.45 K for the (+) cluster up to 3 T. The experimental results are shown in Fig. 6 and 7. As is seen, T_2^{-1} for the (+) cluster (upper branch) decrease monotonously with increasing field down to the field at which T_2^{-1} reaches the value of around 150 s^{-1} . This value is nearly close to the constant value obtained at very low temperature in the temperature dependence of T_2^{-1} . The field dependence at 1.45 K is slightly remarkable than that for 1.65 K. The anomalous peak around $H_0 = 6.8\text{ T}$ in T_2^{-1} may be due to cross-relaxation with ^1H NMR. It should be noted that the field dependence of T_1^{-1} is slightly more remarkable than that of T_2^{-1} . For the (-) cluster (lower branch), on the other hand, the values of T_2^{-1} increase with increasing field. However, the change is rather monotonous as in the case of the (+) cluster. No any appreciable change was observed at the level-crossing fields around $H_0 = 0, 0.45$, and 0.9 T . Figure 8 represents the field dependence of T_2^{-1} for Mn^{4+} ion ($\text{Mn}(1)$) and for Mn^{3+} ion ($\text{Mn}(2)$) for the (+) cluster obtained at 1.45 K. No appreciable difference was found.

IV. ANALYSIS

In this section, we shall analyze the experimental results. The nuclear magnetic relaxations in Mn_{12}Ac will be primarily caused by the fluctuating component $\delta\mathbf{S}(t)$ of the on-site manganese ion via the hyperfine interaction $\delta\mathcal{H}_N(t) = \mathbf{I} \cdot \mathbf{A} \cdot \delta\mathbf{S}(t)$, where \mathbf{A} is the hyperfine interaction tensor given by Eq. 7. In view of the fact that an assembly of the strongly-coupled manganese spins in a cluster is established as the cluster spin of $S = 10$, we may assume that each manganese spin is subject to the same fluctuation corresponding to thermal fluctuation of the cluster spin along the z -axis, which is caused by the spin-phonon interaction. Then, the effective perturbing hyperfine interaction is expressed as

$$\delta\mathcal{H}_N(t) = (I_x A_{xz} + I_y A_{yz} + I_z A_{zz}) \delta S_z(t). \quad (9)$$

Lascialfari *et al.* treated the fluctuating local field due to the spin-phonon interaction in analyzing the proton and muon spin-lattice relaxation rates in Mn_{12}Ac by considering all of Zeeman levels with statistical weight.¹⁸ Here, we simplify the problem by taking into account only the lowest two energy-levels of $S = 10$ within each of the double-well potential, that is, the ground-state $S_z = m = -10$ and the first excited state $m = -9$ for the (+) cluster, and $m = +10$ and $m = +9$ for the (-) cluster. Such a

simplification is reasonable since the present ^{55}Mn NMR is available only at low temperatures below about 2.5 K where the statistical weights of the higher excited states are quite small. Then the average life-times τ_0 and τ_1 of the ground-state and the excited state are given as follows within the framework of the lowest two levels;

$$\frac{1}{\tau_0} = \frac{C\Delta^3}{\exp(\Delta/T) - 1} \quad (10a)$$

and

$$\frac{1}{\tau_1} = \frac{C\Delta^3}{1 - \exp(-\Delta/T)}, \quad (10b)$$

where C is the coupling constant for the spin-phonon interaction,³⁰ and Δ is the energy difference between the ground-state and the first excited state, which is given by

$$\Delta = 19D_I/k_B \pm g_{\parallel}\mu_B H_0/k_B.$$

Here the signs \pm correspond to the upper and lower branches for Mn^{4+} ion, respectively, and vice versa for Mn^{3+} ion. By using the values of $D/k_B = 0.67\text{ K}$,²⁴ and $g_{\parallel} = 1.93$,²⁴ Δ is given as $(12.7 \pm 1.30 \times H_0)\text{ K}$, H_0 being expressed in T. In our present experimental condition for the applied field, the attained value of Δ is at the least about 11 K. So, for the low temperatures below 2.5 K, it turns out, from the expressions given by Eqs. (10), that τ_0 exhibits very remarkable temperature dependence, whereas τ_1 remains almost constant with the relation such that $\tau_0 \gg \tau_1$. Then, the effective fluctuation at each of the ^{55}Mn sites is regarded to be step-wise, and it is characterized by random sudden jumps between the ground-state and the excited state, as shown schematically in Fig. 9. Here h_{α} ($\alpha = z$ or \perp) is the average magnitude of the effective fluctuating field along or perpendicular to the z -axis. These effective fluctuating fields are related to the components of the hyperfine interaction tensor A as $h_z = -A_{zz}/\gamma_N\hbar$ and $h_{\perp} = -A_{xz}/\gamma\hbar$. In the followings we find expressions for the nuclear magnetic relaxation rates on the basis of the above model to look at the experimental results.

A. Transverse relaxation rate

First we consider the transverse relaxation rate. In our experiment, the relaxation time T_2 was determined by measuring the time constant of the decay of the spin-echo amplitude $E(2\tau)$, that is, the macroscopic transverse nuclear magnetic moment, as a function of time interval τ between the two rf -pulses. This decay, which corresponds to the phase disturbance of the Larmor precessions caused by the longitudinal fluctuating local field, is represented as³¹

$$E(2\tau) = E_0 \left\langle \exp \left[i \int_0^{\tau} \delta\omega(t)dt - i \int_{\tau}^{2\tau} \delta\omega(t)dt \right] \right\rangle \quad (11)$$

The spin-echo amplitude can be calculated from Eq. (11) by considering all possible pulse sequences of e fluctuations, the phase deviations and the statistical weight of the pulse sequence. This problem has been treated by Kohmoto *et al.* for the interpretation of ^{133}Cs relaxation times T_2 and T_1 in the $S = 1/2$ Ising-like linear chain antiferromagnet CsCoCl_3 .³² According to the procedure presented in Ref. 32, we obtain, for $\tau_0 \gg \tau_1$, the following final expression

$$E(2\tau) = E_0 \exp\left(-\frac{2\tau}{T_2}\right)$$

with

$$\frac{1}{T_2} = \frac{1}{\tau_0} \cdot \frac{(\gamma_N h_z \tau_1)^2}{1 + (\gamma_N h_z \tau_1)^2}. \quad (12)$$

Thus the relaxation rate depends on the number of the fluctuation pulse per second, τ_0^{-1} and average phase change $\gamma_N h_z$ for one fluctuating field. The above equation yields for $\gamma_N h_z \tau_1 \ll 1$

$$\frac{1}{T_2} = \frac{1}{\tau_0} (\gamma_N h_z \tau_1)^2 \sim \frac{\tau_1^2}{\tau_0}, \quad (13a)$$

and for $\gamma_N h_z \tau_1 \gg 1$

$$\frac{1}{T_2} = \frac{1}{\tau_0}. \quad (13b)$$

As we see in the following section, Eq. (13a) corresponds to the expression obtained on the basis of the standard perturbation method, that is, the weak collision regime. On the other hand, Eq. (13b) means that the relaxation rate is determined solely by the average number of the appearance of the thermal excitation per one second, and further it does not depend on the magnitude of the fluctuating field. This is the strong collision regime. As evaluated above, in the present experimental conditions, the temperature dependence of T_2^{-1} results predominantly through the term of τ_0 . Accordingly, as far as the temperature dependence is concerned, there is no appreciable difference between both regimes for T_2^{-1} . On the other hand, since the term of Δ^3 in τ_0 and τ_1 contributes to the field dependence of T_2^{-1} , the qualitative difference between Eqs. (13a) and (13b) is expected to appear in the field dependence of T_2^{-1} . Thus it is worthwhile to look at the qualitative field dependence of T_2 to find the plausible regime. The field-dependence of the relevant terms of τ_0 and $\tau_1^2 \tau_0^{-1}$ calculated for $T=1.45\text{ K}$ are shown in Fig. 10 by the solid and dashed lines, respectively. Clearly the solid line in Fig. 10, which represents τ_0^{-1} , explains well the corresponding experimental curve given in Fig. 6. This means that the strong-collision regime is valid. The solid line in Fig. 5 represents the result for qualitative fitting of the calculated curve of Eq. (13b) for zero field to the experimental temperature dependence of T_2^{-1} . It should be noted that there appears no definite dependence of T_2^{-1} on the site of the

manganese nuclei, although there exists rather large difference in the A_{zz} component of the hyperfine tensor as estimated in the previous section (see Eqs. (7)). This is well understood if we adopt Eq. (13b). The results for the similar fittings for the field dependence of T_2^{-1} are shown in Fig. 6 by the solid and dotted lines. The solid line in Fig. 8 represents the fitted curve of Eq. (13b). In both cases of the temperature and field dependence of T_2^{-1} , the agreements are satisfactory. Thus it is concluded that the transverse relaxation is essentially determined by the phase disturbance associated with the average number of the appearance of the first excited state per one second (strong collision regime).

B. Longitudinal relaxation rate

Now let us turn to the longitudinal relaxation rate. If we pay attention to the experimental fact that $T_2^{-1} \gg T_1^{-1}$ together with the validity of Eq. (13b), it is reasonable to assume that the longitudinal relaxation time T_1 is much longer than the characteristic times τ_0 and τ_1 . Then, the longitudinal relaxation rate T_1^{-1} should be obtained, following to the conventional perturbation theory, by the spectral component at the ^{55}Mn Larmor frequency ω_N of the time correlation function for the step-wise fluctuating field as given in Fig. 9. The time correlation function for such a fluctuating field is easily calculated to be

$$\langle \{h_+(t)h_-(0)\} \rangle = h_{\text{eff}}^2 \exp(-\frac{t}{\tau_c}) \quad (14)$$

with

$$h_{\text{eff}}^2 = \frac{\tau_0\tau_1}{(\tau_0 + \tau_1)^2} h_{\perp}^2 \approx \frac{\tau_1}{\tau_0} h_{\perp}^2 \quad (15)$$

and

$$\frac{1}{\tau_c} = \frac{1}{\tau_0} + \frac{1}{\tau_1} \approx \frac{1}{\tau_1}, \quad (16)$$

where τ_c is the correlation time. The approximation used in Eqs. (15) and (16) is valid under the condition that $\tau_0 \gg \tau_1$, which is the relevant case. Taking the Fourier transform of Eq. (14), we obtain for $\tau_0 \gg \tau_1$,

$$\frac{1}{T_1} = \frac{\tau_1}{\tau_0} (\gamma_N h_{\perp})^2 \frac{2\tau_1}{1 + (\omega_N \tau_1)^2}. \quad (17)$$

This equation yields for $\omega_N \tau_1 \ll 1$

$$\frac{1}{T_1} = \frac{2(\gamma_N h_{\perp} \tau_1)^2}{\tau_0} \sim \frac{\tau_1^2}{\tau_0}, \quad (18a)$$

and for $\omega_N \tau_1 \gg 1$

$$\frac{1}{T_1} = \frac{2(\gamma_N h_{\perp})^2}{\tau_0 \omega_N^2} \sim \frac{1}{\tau_0 \omega_N^2}. \quad (18b)$$

Here the resonance frequency is given by $\omega_N = \gamma_N(H_{\text{int}} \pm H_0)$, where the signs \pm correspond to the upper and lower

branches for Mn^{4+} ion and vice versa for Mn^{3+} ion. As in the case of T_2^{-1} , the temperature dependence of T_1^{-1} is almost determined by τ_0 , while the field dependence depends not only on τ_0 but also on τ_1^2 and ω_N^2 . The field dependence of T_1^{-1} is determined by $\tau_1^2 \tau_0^{-1}$ for the low-frequency limit $\omega_N h_z \tau_1 \ll 1$, and by $\tau_0^{-1} \omega_N^{-2}$ for the high-frequency limit $\omega_N h_z \tau_1 \gg 1$. The dotted line in Fig. 10 represents the field dependence of $\tau_0^{-1} \omega_N^{-2}$ calculated for $T = 1.45$ K. It is found that the experimental field dependence obtained for $T = 1.45$ K fits well the dotted line, but not the dashed line, thus suggesting the validity of the equation for the high-frequency limit instead of the other. The dot-dashed and dotted lines in Fig. 5 represent the results of the best fitting of the curve τ_0^{-1} for zero field to the experimental results for temperature dependence for the L1-line (Mn^{4+} ion) and the L2-line (Mn^{3+} ion). The agreement is reasonable down to around 0.7 K. The results for the similar fittings for the field dependence of T_1^{-1} are shown in Fig. 6 by the solid and dotted lines. The agreement is also satisfactory. Thus it turns out that the longitudinal relaxation is governed by perturbing effect of the fluctuating field $h_{\perp}(t)$ (weak collision model), and then the high-frequency limit for the ω_N component of the correlation function of $h_{\perp}(t)$ holds. It should be noted that the slight difference in the field dependence between T_2^{-1} and T_1^{-1} results from the presence of the factor ω_N^{-2} in the latter, which is approximated as $(\gamma_N H_{\text{int}})^{-2} (1 - 2H_0/H_{\text{int}})$ for $H_{\text{int}} \gg H_0$.

V. DISCUSSIONS

First we examine the above treatment numerically. The use of T_2 yields directly the value of τ_0 . Then we obtain the constant for the spin-phonon interaction, $C \approx 5 \times 10^3 \text{ s}^{-1} \text{ K}^{-3}$, which lies reasonably in the range of the value of $10^3 \sim 10^5 \text{ s}^{-1} \text{ K}^{-3}$ predicted in Ref. 3. Using this value, we obtain $\tau_1 \approx 1.1 \times 10^{-7} \text{ s}$. Here if we tentatively assume that the deviation of the cluster spin of $\delta S_z = 1$ during τ_1 is shared by the 12 manganese spins, the average deviation of each spin is taken to be $\delta S_z = 1/4$. Then, for instance, the use of $A_{zz}/\hbar = 154 \text{ MHz}$ for Mn^{4+} ion yields $\gamma_N h_z \tau_1 \approx 25$, thus the condition for the strong collision regime for T_2^{-1} relaxation process being satisfied. The reason why there appears above about 2 K the slight difference in the value of T_2^{-1} between Mn^{4+} and Mn^{3+} ions might be due to the cross-over from the strong-collision regime to the weak collision regime. In fact, in the latter, the difference in the coupling constant term, that is, $\gamma_N h_z$ or A_{zz}/\hbar should reflect in the value of T_2 . Nevertheless, as far as we are confined ourselves within the present simplified treatment, it is not realized because τ_1 is almost temperature-independent.

As for T_1 , for instance, using the evaluated value of $A_{zz}/\hbar = 24.7 \text{ MHz}$ ($\text{Mn}(2)$) and 53 MHz ($\text{Mn}(3)$), we obtain $T_2^{-1}/T_1^{-1} \approx 500$ and 100 , respectively, which agrees reasonably with the experimental result in relative order of magnitude. However, the following points remain not

understood. First, as far as the hyperfine interaction for Mn^{4+} ion is taken to be isotropic and not to have off-diagonal terms as determined in the present analysis of the NMR spectra, it is difficult to understand that the relaxation rate for Mn^{4+} ion is of comparable order with that for Mn^{3+} ion. In order to understand the experimental results for T_1 for Mn^{4+} ion, the assumption of the presence of any off-diagonal term of the hyperfine interaction tensor will be necessary. Unless the anisotropic term is not effective, the possible relaxation mechanism may be inevitably ascribed to the isotropic interaction term like $AI^+\delta S^-(t)$ as in the case of the three-magnon relaxation process in usual magnetic system. In this case, the relevant activation energy which determines the temperature dependence of T_1 should be at least twice of the gap energy so as to guarantee the energy conservation between the nuclear spin and the electronic spin system. However, in the cluster which involves only twelve electronic spins coupled strongly to each other by exchange interactions, it may be quite unreliable. Anyhow, the origin of the effective coupling constant for T_1 for Mn^{4+} ion is uncertain at the present.

Next we discuss on the present concept for obtaining the relevant equations for T_2 and T_1 . As a starting point we considered only the two lowest levels, the ground-state and the first excited state. Then, if we follow the standard stochastic theory, the fluctuating local field responsible for the nuclear magnetic relaxation, which is caused by the thermal excitation to the excited state from the ground-state, is treated as a perturbation with respect to the nuclear quantization axis. In the cases of zero field and where the external field is applied along the c -axis, the nuclear quantization axis is taken to be along the internal field at the ^{55}Mn site, that is, along the c -axis. The longitudinal and transverse relaxation rates are given by the Fourier spectrum of correlation function of such a fluctuating local field $h_\alpha(t)$ ($\alpha = z$ or \perp) at the resonance frequency ω_N as follows:

$$\frac{1}{T_1} = F_\perp(\omega_N) \quad \text{and} \quad \frac{1}{T_2} = \frac{1}{2T_1} + F_z(0)$$

with

$$F(\omega_N) = \frac{\gamma_N^2}{2} \int_{-\infty}^{\infty} \langle \{ \delta h_\alpha(t) \delta h_\alpha(t) \} \rangle \exp(-i\omega_N t) dt. \quad (19)$$

As shown in Sec. IV, the correlation function for the pulse-like field given in Fig. 9, is calculated to have the exponential-typed form given by Eq. (14). The longitudinal relaxation rate has already been given by Eq. (17). On the other hand, we have found experimentally that $T_2^{-1} \gg T_1^{-1}$. So T_2^{-1} should be ascribed to the zero-frequency term $F(0)$, which is given by

$$\frac{1}{T_2} = F(0) = \frac{\tau_1^2}{\tau_0} (\gamma_N h_z)^2. \quad (20)$$

According to this equation, the temperature dependence of T_2^{-1} results only from τ_0 as far as $\tau_0 \gg \tau_1$ because

τ_1 is taken to be almost independent on the temperature. However, the value of T_2^{-1} should have a large site-dependence through the coupling constant term $(\gamma_N h_z)^2$, which is proportional to the hyperfine interaction term of A_{zz}^2 . Furthermore, as already shown in Fig. 10, the field dependence of $\tau_1^2 \tau_0^{-1}$ differs from that of only τ_0^{-1} . Such features contradict with our experimental results. Instead, as we have already mentioned, the equation like $T_2^{-1} = \tau_0^{-1}$ obtained as a strong collision regime on the basis of more basic treatment explains satisfactorily our experimental results for T_2 .

Finally, with respect to the longitudinal relaxation, we compare our present formalism with the equation adopted by Furukawa *et al.* in Ref. 19. They have taken into account all of the 21 energy levels ($m = -10 \sim +10$) of $S = 10$ as the candidates for the fluctuating field δh_\perp responsible for the nuclear magnetic relaxation. Then, it has been assumed that the correlation functions associated with each of these energy levels are the exponential-typed one with the correlation time equal to the corresponding average life time, which is determined by the spin-phonon interaction as discussed in Ref. 3. The contributions from each level have been summed up with the statistical weight. However, in considering the low temperature results, only the term related to the lowest ground-state with $m = -10$ with the predominant statistical weight was remained as an effective one, thus yielding the expression like $T_1^{-1} \propto A_\pm^2 / \tau_0 \omega_N^2$ in the high-frequency limit for $\tau_0 \omega_N \gg 1$. As is seen, our equation (18b) has the same form as this equation. However, the origins of each term are different. First, in Eq. (18b), the term τ_0 results from the effective amplitude of the fluctuating field $(\tau_1/\tau_0)(\gamma_N h_\perp)^2$ in the correlation function. Secondly the criterion for the high-frequency limit, which brings the term ω_N in the equation, is taken with respect to $\tau_1 \omega_N$ instead of $\tau_0 \omega_N$. Thirdly, as for the coupling constant, Eq. (18b) involves the transverse fluctuating field h_\perp , that is, the off-diagonal term A_{xz} , since it is assumed that the anisotropic perturbing interaction like $I^+ \delta S_z(t)$ is responsible for the nuclear spin lattice relaxation. While, in Ref. 19, the coupling constants for $\text{Mn}(1)$, $\text{Mn}(2)$, and $\text{Mn}(3)$ have been taken to be proportional to the square of the internal static field in zero field, *i. e.*, square of A_{zz} in our notation. Then, in view of the large difference of the ratio of the coupling constants of T_1^{-1} for the three ions between experimental values and the above estimation, the presence of the coupling constants for non-zero mode have been suggested. Unfortunately the ^{55}Mn NMR signal is observable only at low temperatures. So it is difficult to find experimentally the maximum point of the relaxation rate which appears in the BPP-typed equation under the condition $\tau_1 \omega_N = 1$. It may be possible for other nuclei with much lower resonance frequency. However, such a condition is realized at rather high temperatures. In this case, the present two-level model may fail. Further extension of the present treatment will be necessary by taking into account the higher excited levels.

VI. CONCLUSION

The nuclear magnetic relaxation times T_2 and T_1 of ^{55}Mn for Mn^{4+} and Mn^{3+} ions in Mn_{12}Ac have been measured using the oriented powder sample at low temperatures below 2.5 K down to 200 mK in the fields up to 9 T applied along c -axis. The relaxation rates T_2^{-1} and T_1^{-1} in zero field exhibited remarkable decreases with decreasing temperature with the relative relation like $T_2^{-1}/T_1^{-1} = 200$ at the temperatures above about 1.5 K. At the lower temperatures the difference was more pronounced. The field dependence of T_2^{-1} and T_1^{-1} showed decrease with increasing field for the cluster whose magnetic moment is parallel to the c -axis. On the contrary, those for the cluster whose magnetic moment is antiparallel to the c -axis increase with increasing field. The analysis for the experimental results was made on the concept that the nuclear magnetic relaxation is caused by thermal excitations of the cluster spin. We simplified the problem by considering only the excitation from the ground-state to the first excited state within each well of the double-well potential with the average life times determined by the spin-phonon interaction. On basis of the nonlinear theory, we obtained general expression for the transverse

relaxation rate T_2^{-1} for such a pulse-like fluctuating field. It turned out that T_2^{-1} is well understood in terms of the equation $T_2^{-1} = \tau_0^{-1}$, which corresponds to the strong collision regime. On the other hand, the experimental results for T_1^{-1} was interpreted well by the standard perturbation formalism. On the other hand, the results for T_1 have been well understood, on the basis of the standard perturbation method, by the equation for the high-frequency limit like $T_1^{-1} \sim 1/\tau_0\omega_N^2$, where ω_N is the ^{55}Mn Larmor frequency. The quantitative comparison between the experiment and the theoretical calculation was made by using the ^{55}Mn hyperfine interaction tensors, which resulted in reasonable agreement.

Acknowledgments

The authors wish to thank Professor T. Kohmoto for valuable discussions. Discussions with Professor F. Borsa and Dr. A. Lascialfari are greatly appreciated. Thanks are also due to Dr. Y. Furukawa for giving us useful informations. This work is supported by the Grant-in-Aid for Scientific Research from Ministry of Education, Culture, Sports, and Technology.

-
- * Electronic address: goto@nmr.jinkan.kyoto-u.ac.jp
† Present address: Toshiba Corporation, Semiconductor Company, 8 Shinsugimoto-cho, Isogo-ku, Yokohama, 235-8522, Japan
- ¹ T. Lis, *Acta. Cryst.* **B36**, 2042 (1980).
 - ² R. Sessoli, D. Gatteschi, A. Caneschi, and M. A. Novak, *Nature* **365**, (1993).
 - ³ J. Villain, F. Hartmann-Boutron, R. Sessoli, and A. Petti, *Europhys. Lett.* **27**, 159 (1994).
 - ⁴ L. Thomas, F. L. Lioni, R. Ballou, D. Gatteschi, R. Sessoli, and B. Barbara, *Nature* **383**, 145 (1996).
 - ⁵ J. R. Friedman, M. P. Sarachik, J. Tejada, and R. Ziolo, *Phys. Rev. Lett.* **76**, 3830 (1996).
 - ⁶ P. Politi, A. Rettori, F. Hartmann-Boutron, and J. Villain, *Phys. Rev. Lett.* **75**, 537 (1995).
 - ⁷ C. Sangregorio, T. Ohm, C. Paulsen, R. Sessoli, and D. Gatteschi, *Phys. Rev. Lett.* **78**, 4645 (1997).
 - ⁸ W. Wernsdorfer, R. Sessoli, and D. Gatteschi, *Science* **184**, 133 (1999).
 - ⁹ I. Chiorescu, W. Wernsdorfer, A. Müller, H. Bogge, and B. Barbara, *Phys. Rev. Lett.* **84**, 3454 (2000).
 - ¹⁰ L. Gunther and B. Barbara, *Quantum Tunneling of Magnetization* (Kluwer, Dordrecht, 1995).
 - ¹¹ E. M. Chudnovsky and J. Tejada, *Macroscopic Quantum Tunneling of Magnetic Moment* (Cambridge University Press, Cambridge, 1997).
 - ¹² F. Hartmann-Boutron, P. Politi, and J. Villain, *J. Mod. Phys.* **B21**, 2577 (1996).
 - ¹³ L. Tupitsyn and N. V. P. and P. C. E. Stamp, *J. Mod. Phys.* **B11**, 2901 (1997).
 - ¹⁴ I. Tupitsyn and B. Barbara, *Quantum tunneling of magnetization in molecular complexes with large spins. Effect of the environment.*, *cond-mat/0002180*.
 - ¹⁵ T. Goto, T. Kubo, T. Koshiba, Y. Fujii, A. Oyamada, J. Arai, K. Takeda, and K. Awaga, *Physica B* **284**, 1277 (2000).
 - ¹⁶ T. Kubo, T. Goto, T. Koshiba, K. Takeda, and K. Awaga, *Phys. Rev. B* **65**, 224425 (2002).
 - ¹⁷ A. Lascialfari, D. Gatteschi, F. Borsa, A. Shastri, Z. H. Jang, and P. Carretta, *Phys. Rev. B* **57**, 514 (1998-I).
 - ¹⁸ A. Lascialfari, Z. H. Jang, F. Borsa, P. Carretta, and D. Gatteschi, *Phys. Rev. Lett.* **81**, 3773 (1998).
 - ¹⁹ Y. Furukawa, K. Watanabe, K. Kumagai, F. Borsa, and D. Gatteschi, *Phys. Rev. B* **64**, 104401 (2001).
 - ²⁰ T. Koshiba, T. Goto, T. Kubo, and K. Awaga, *Prog. Theor. Phys. Suppl.* **145**, 2002 (2002).
 - ²¹ R. Sessoli, H. L. Tsai, A. R. Schake, S. Wang, J. B. Vincent, K. Folting, D. Gatteschi, G. Christou, and D. N. Hendricson, *J. Am. Chem. Soc.* **115**, 1804 (1993).
 - ²² A. Caneschi, D. Gatteschi, R. Sessoli, A. L. Barra, L.-D. Brunel, and M. Guillot, *J. Am. Chem. Soc.* **113**, 5873 (1991).
 - ²³ N. Regnault, T. Jolicœur, R. Sessoli, D. Gatteschi, and M. Verdager, *Exchange couplings in the magnetic molecular cluster Mn_{12}Ac* , *cond-mat/0203480*.
 - ²⁴ A. L. Barra, D. Gatteschi, and R. Sessoli, *Phys. Rev. B* **56**, 8192 (1997).
 - ²⁵ I. Mirebeau, M. Hennion, H. Casalta, H. Andres, H. U. Gudel, A. V. Irodova, and A. Caneschi, *Phys. Rev. Lett.* **83**, 628 (1999).
 - ²⁶ T. Pohjola and H. Schoeller, *Phys. Rev. B* **62**, 15026 (2000-II).
 - ²⁷ A. J. Freeman and R. E. Watson, *Magnetism IIA*, edited by T. Rado and H. Shull (Academic Press, New York, 1965).
 - ²⁸ A. Robinson, P. J. Brown, D. N. Argyriou, D. N. Hendrikson, and M. J. Aubin, *J. Phys. B* **12**, 2805 (2000).

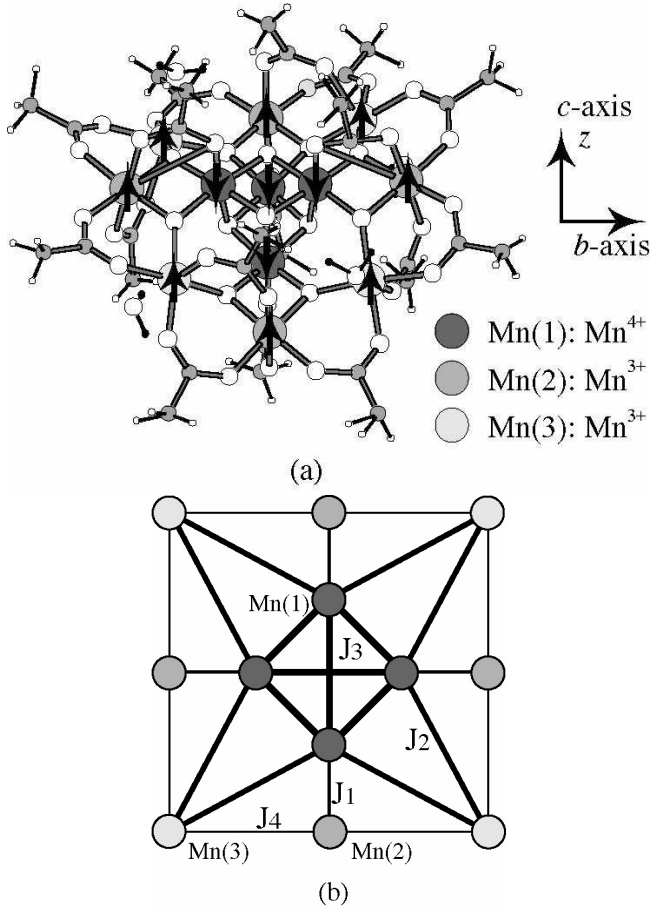


FIG. 1: Crystal Structure of molecular cluster of Mn_{12}Ac . The crystalline c -axis (the z -axis), along which the structure is viewed, is taken to tilt upward from the surface of the text. The deeply and lightly shaded large circles represent Mn^{4+} ion and Mn^{3+} ions, respectively. The shaded and open circles, and the small closed circles represent carbon, oxygen, and proton of water molecule, respectively. The arrows on each of the manganese sites indicate the directions of the magnetic moments which are parallel or antiparallel to the c -axis. (b) Schematic drawing of the exchange interactions among the manganese ions, J_i ($i = 1, \dots, 4$), whose values are referred to the text.

- ²⁹ P. W. Andrew and D. P. Tunstall, Proc. Phys. Soc. **78**, 1 (1961).
- ³⁰ J. Villan, F. H. Boutron, R. Sessoli, and A. Rettori, Euro. Phys. Lett. **27**, 159 (1994).
- ³¹ J. R. Klander and P. W. Anderson, Phys. Rev. **125**, 912 (1962).
- ³² T. Kohmoto, T. Goto, S. Maegawa, N. Fujiwara, Y. Fukuda, M. Kunitomo, and M. Mekata, Phys. Rev. B **49**, 6028 (1994).

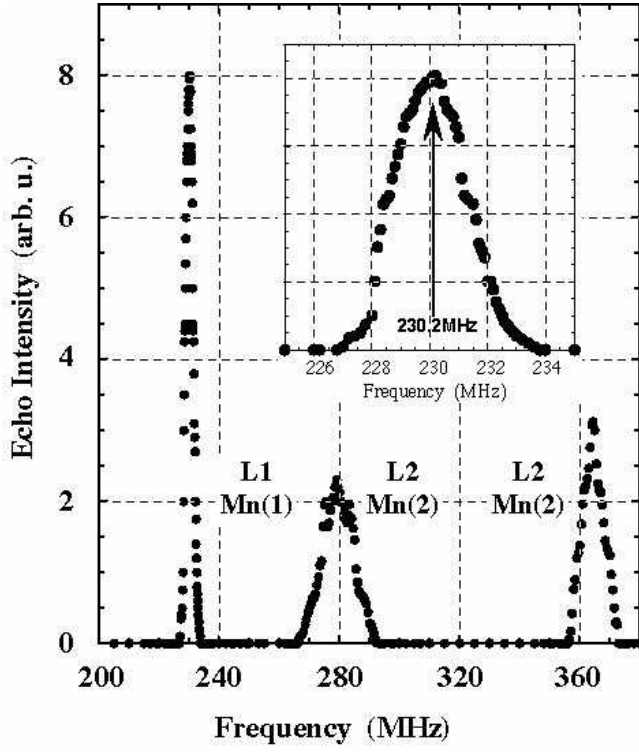


FIG. 2: ^{55}Mn NMR spectra in Mn_{12}Ac obtained at 1.4 K in zero field. The three resonance lines labeled by L1, L2, and L3 are associated with Mn^{4+} (Mn(1)), and two inequivalent Mn^{3+} ions (Mn(2) and Mn(3)), respectively. The inset shows the detail of the L1 line.

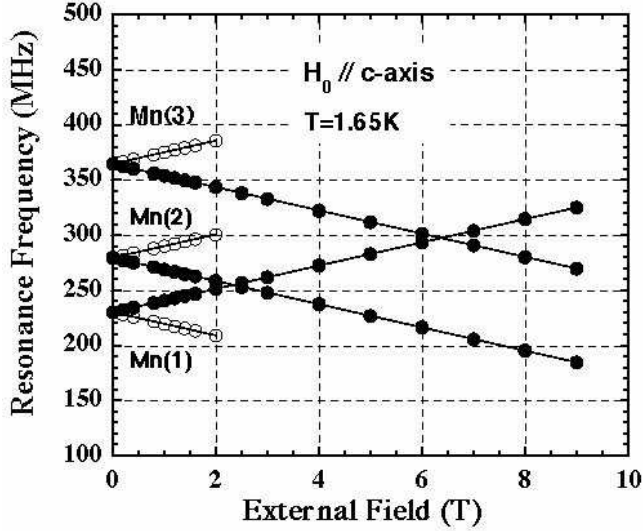


FIG. 3: The field dependence of the resonance frequencies of the central peak of the three resonance lines L1, L2, and L3 obtained at 1.65 K. The external field is applied along the c -axis. The closed and open circles correspond to the ^{55}Mn NMR belonging to the (+) and (-) clusters, respectively.

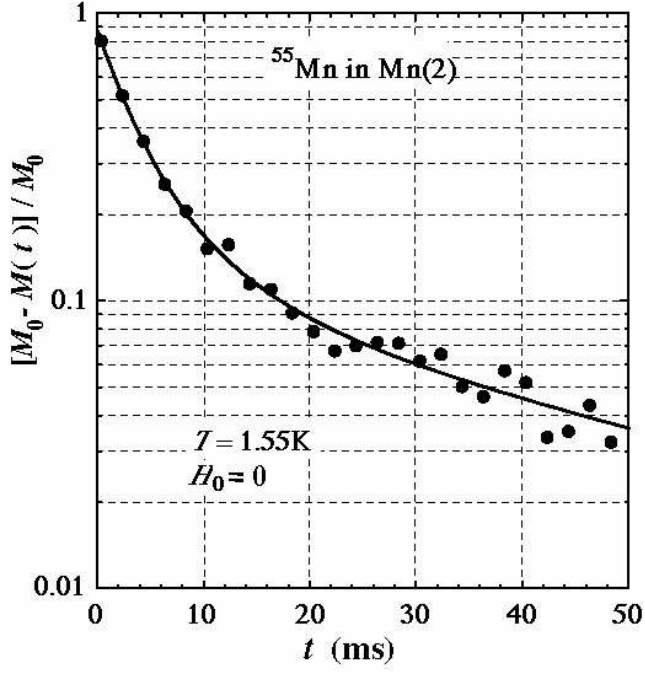


FIG. 4: A typical example of the recovery of the ^{55}Mn nuclear magnetization $M(t)$ measured for $\text{Mn}(2)$ at $T = 1.55\text{K}$ in zero field as a function of the time t between the end of the saturation rf -pulse and the beginning of the searching rf -pulse, which is normalized with the equilibrium value M_0 . This is a fitting curve shown by the solid line yields $T_1 = 44.7\text{ms}$ using the best fit values of the coefficients $a = 0.11$, $b = 0.24$, and $c = 0.51$ in Eq. (8).

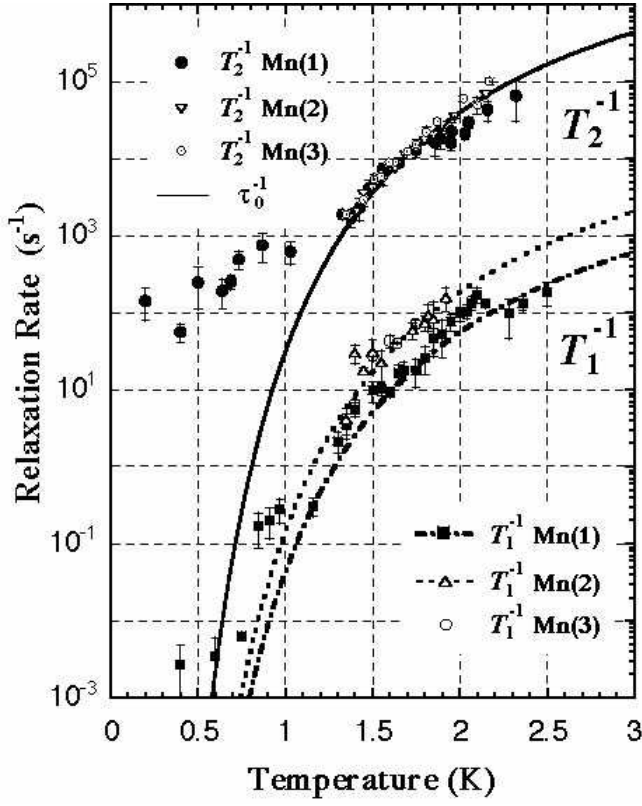


FIG. 5: Temperature dependence of T_2^{-1} and T_1^{-1} of ^{55}Mn for Mn^{4+} ion (Mn(1)) and Mn^{3+} ions (Mn(2) and Mn(3)) in zero field. The solid line represents the temperature dependence of τ_0^{-1} (Eq. (13b)). The dot-dashed and dotted lines represent the best fit of Eq. (18b) to the experimental results for Mn^{4+} ion and for Mn^{3+} ion (Mn(2)), respectively. The temperature dependence of Eq. (18b) is given by τ_0^{-1} .

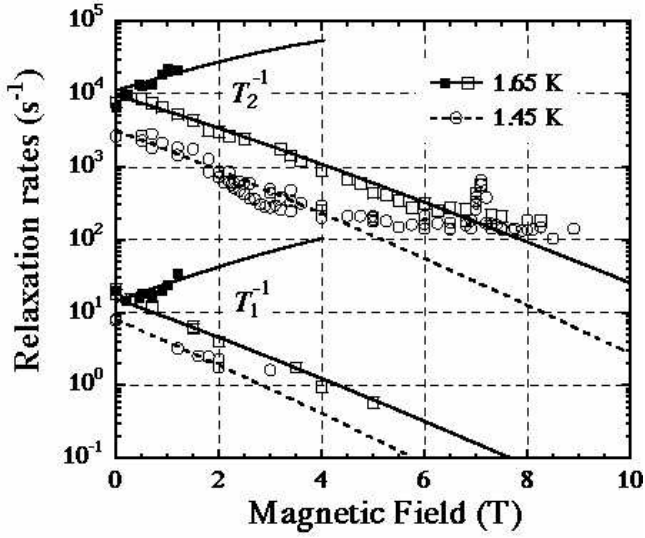


FIG. 6: Field dependence of T_2^{-1} and T_1^{-1} for the L1 line (Mn^{4+} ion). The external field is applied along the c -axis. The open and closed squares represent the experimental results obtained at 1.65 K for the upper branch ((+) cluster) and the lower branch ((-) cluster), respectively. The open circles represent the experimental results for the upper branch obtained at 1.45 K. The solid and dashed lines drawn for the results of T_2^{-1} represent the theoretical equations of τ_0^{-1} corresponding at 1.65 and 1.45 K, respectively. Those for the results of T_1^{-1} represent the best-fit of the theoretical equations of $\tau_0^{-1}\omega_N^{-2}$ to the experimental results.

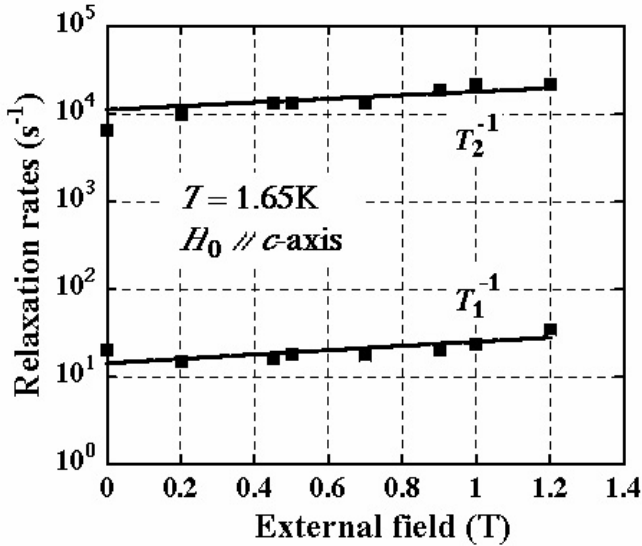


FIG. 7: Field dependence of the relaxation rates T_2^{-1} and T_1^{-1} of ^{55}Mn in Mn^{4+} ion for the the (-) cluster (lower branch) measured at 1.65 K.

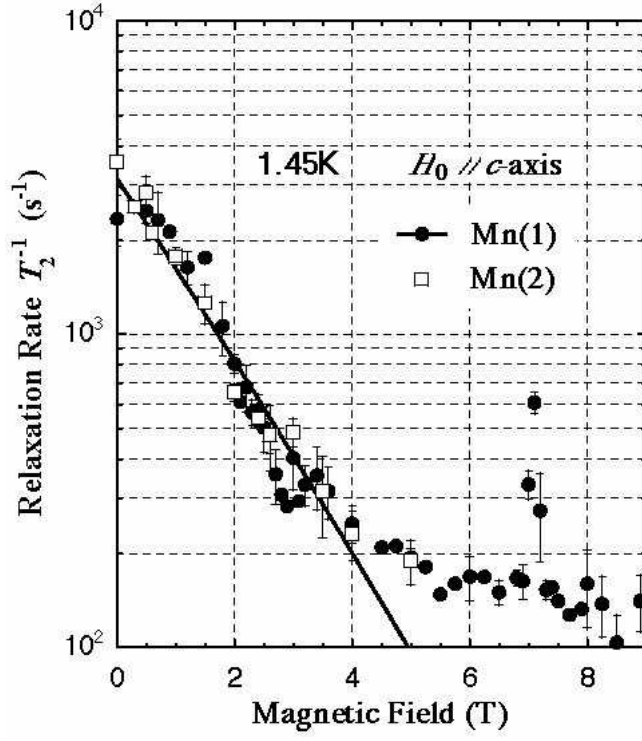


FIG. 8: Field dependence of T_2^{-1} of the ^{55}Mn in Mn(1) and Mn(2) for the(+) cluster obtained at 1.45 K.

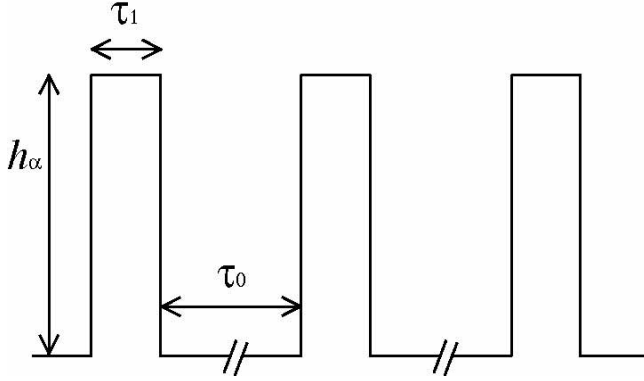


FIG. 9: Schematic drawing of the step-wise fluctuating local field associated with the excitation from the ground-state to the first excited state with respective average life-times of τ_0 and τ_1 . h_α represents the fluctuating field longitudinal ($\alpha = z$) or transverse ($\alpha = \perp$) with respect to the nuclear quantization axis, which coincides to the $c(z)$ -axis.

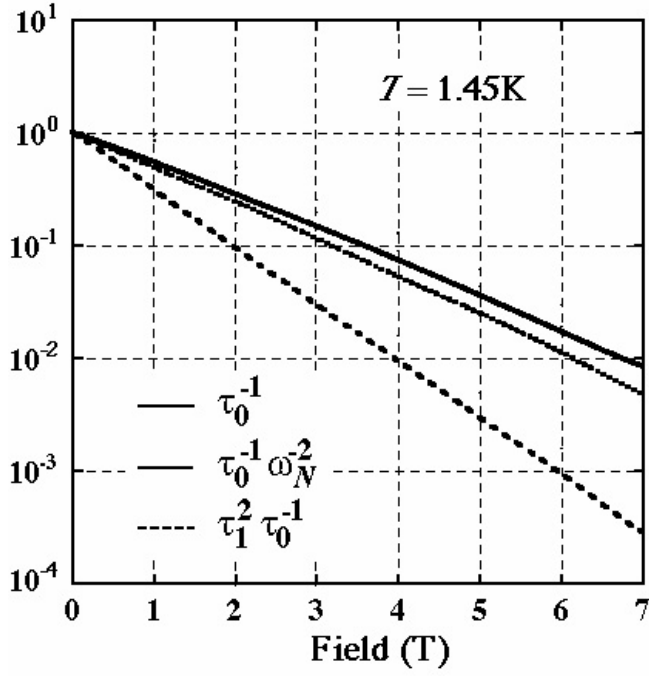


FIG. 10: The qualitative field dependence of the relevant terms in the theoretical equations of the relaxation rates T_2^{-1} and T_1^{-1} calculated for $T = 1.45\text{K}$. The solid and dashed lines represent the field dependence of T_2^{-1} corresponding to the strong- and weak-collision regimes, respectively. The dotted and dashed lines represent the field dependence of T_1^{-1} corresponding to the high- and low-frequency limits, respectively. These curves are normalized at $H_0 = 0$.